Anal Bioanal Chem (2016) 408:4975–4985
DOI 10.1007/s00216-016-9592-y

RESEARCH PAPER

High-throughput and rapid quantification of lipids by nanoflow UPLC-ESI-MS/MS: application to the hepatic lipids of rabbits with nonalcoholic fatty liver disease

Seul Kee Byeon[1] · Jong Cheol Lee[1] · Bong Chul Chung[2] · Hong Seog Seo[3] · Myeong Hee Moon[1]

Received: 2 March 2016 / Revised: 11 April 2016 / Accepted: 20 April 2016 / Published online: 13 May 2016

Abstract A rapid and high-throughput quantification method (approximately 300 lipids within 20 min) was established using nanoflow ultrahigh-pressure liquid chromatography-tandem mass spectrometry (nUPLC-ESI-MS/MS) with selective reaction monitoring (SRM) and applied to the quantitative profiling of the hepatic lipids of rabbits with different metabolic conditions that stimulate the development of nonalcoholic fatty liver disease (NAFLD). Among the metabolic conditions of rabbits in this study [inflammation (I), high-cholesterol diet (HC), and high-cholesterol diet combined with inflammation (HCI)], significant perturbation in hepatic lipidome (>3-fold and $p < 0.01$) was observed in the HC and HCI groups, while no single lipid showed a significant change in group I. In addition, this study revealed a dramatic increase (>2-fold) in relatively high-abundant monohexosylceramides (MHCs), sphingomyelins (SMs), and triacylglycerols (TGs) in both the HC and HCI groups, especially in MHCs as all 11 MHCs increased by larger than 3- to 12-fold. As the levels of the relatively high-abundant lipids in the above classes increased, the total lipidome level of each class increased significantly by approximately 2-fold to 5-fold. Other classes of lipids also generally increased, which was likely induced by the increase in mitogenic and nonapoptotic MHCs and SMs, as they promote cell proliferation. On the other hand, a slight decrease in the level of apoptotic ceramides (Cers) was observed, which agreed with the general increase in total lipid level. As distinct changes in hepatic lipidome were observed from HC groups, this suggests that HC or HCI is highly associated with NAFLD but not inflammation alone itself.

Keywords Hepatic lipid · Inflammation · High-cholesterol diet · Nonalcoholic fatty liver disease · nUPLC-ESI-MS/MS

Introduction

Lipids have regulatory roles in various cellular processes such as membrane structure maintenance, signaling, and apoptosis [1, 2]. Changes in lipid levels are correlated with the pathogenesis and progression of various types of metabolic diseases because the perturbed levels of lipids are directly associated with health risks [3]. Among the various classes of lipids, phospholipids (PLs) are the most abundant in cell membranes, and sphingolipids (SLs) play central roles in cellular growth and modulate the proliferation of cancer cells [4]. As a precursor of all SLs, Cer is converted to other types of SLs by the addition of one or more sugar moieties [5]. Neutral glycerides constitute various fatty acids that are esterified to glycerol, such as diacylglycerides (DGs) and triacylglycerides (TGs).

Although lipid molecules are diverse and structurally complex, the rapid growth in mass spectrometry (MS) and associated techniques over the past decade has facilitated the accurate determination of lipid molecular structures and advanced lipidomics to a prominent research area in metabolomics. Liquid chromatography (LC) with electrospray ionization MS (LC-ESI-MS) has expanded the analytical power of MS

Electronic supplementary material The online version of this article (doi:10.1007/s00216-016-9592-y) contains supplementary material, which is available to authorized users.

✉ Myeong Hee Moon
mhmoon@yonsei.ac.kr

[1] Department of Chemistry, Yonsei University, Seoul 03722, Republic of Korea

[2] Future Convergence Research Division, Korea Institute of Science and Technology, Seoul 02792, Republic of Korea

[3] Cardiovascular Center, Korea University Guro Hospital, Seoul 08308, Republic of Korea

for the qualitative and quantitative profiling of lipids from complicated biological origins because lipid separation and characterization can be achieved for intact lipids, even at trace levels, with good resolving power and reproducibility [6]. The use of nanoflow for lipid separation with capillary columns is especially effective at achieving good resolution of separation and MS detection because nanoflow during ESI generates more ions for the MS analysis and decreases the detection limit to the low femtomole level [7, 8] and solvent consumption. Recently, nanoflow LC-ESI-MS/MS was utilized for the lipidomic analysis of plasma from patients with coronary artery disease [9, 10], urine from prostate cancer patients [11], and the evaluation of both plasma and urine in rare genetic disorders like Gaucher [12] and Fabry [13] diseases after enzyme replacement therapy.

The liver plays a key role in lipid synthesis and is actively involved in various metabolic processes (e.g., removing toxins and processing nutrients from food). In response to feeding and fasting, fatty acids and TGs actively flow in and out of the liver. The accumulation of hepatic TGs causes fatty liver, or steatosis [14], which can progress to fatty liver disease (FLD). While the conventional etiological entity of FLD is alcohol consumption, obesity along with a number of metabolic etiologies [15, 16] has been reported to cause FLD development. The latter case is referred to as nonalcoholic FLD (NAFLD) which is indicated by an abnormal accumulation of hepatic TGs with an overexpression of hepatic PPARγ, a crucial regulator of fatty acid uptake and TG synthesis [17], and a decrease of free acid oxidation [18]. Approximately 75 % of individuals with obesity are diagnosed with hepatic steatosis, and 35 % of these are likely to develop NAFLD. Simple NAFLD may be benign and hardly fatal, without any clear symptoms that alarm at-risk patients; however, it can lead to serious complications such as steatohepatitis when inflammation is present [19]. Inflamed fatty liver can harden over time, resulting in cirrhosis, liver scarring, and liver damage or cancer [20, 21]. NAFLD is reportedly related to obesity, hypertension, insulin resistance, and hyperlipidemia. As elevated hepatic TG level is the hallmark of NAFLD, most of the published studies on NAFLD focused on TGs [22], and a few have characterized other classes of lipids (e.g., DGs) that increased dramatically under NAFLD; however, only a handful of lipids (approximately ≤100 lipids) have been analyzed [23, 24]. Thus, investigations of comprehensive lipidome from the liver and evaluations of specific types of lipids that are affected and their degree in alteration need to be conducted.

In this study, we investigated alterations in hepatic lipidome profiles in rabbits with different metabolic conditions that lead to NAFLD: inflammation (I) induced by feeding carrageenan, high-cholesterol diet (HC), and high-cholesterol diet in combination with inflammation (HCI). High-cholesterol levels and inflammation have been reported as risk factors for the development of metabolic syndrome and particularly NAFLD because high-cholesterol diets promote the accumulation of fats and lipids on various organs throughout the body [25]. For the global search of lipids from liver tissue, pooled samples of hepatic tissue were first analyzed by nLC-ESI-MS^n using an ion trap mass spectrometer, and the identified lipids were then rapidly quantified from individual samples by nUPLC-ESI-MS/MS using a triple-quadrupole mass spectrometer. For the latter, a high-throughput (>300 lipids) relative quantitation method based on selective reaction monitoring (SRM) responses was established for the high-speed separation (<20 min per sample) using nanoflow (300 nL/min), which enhances reliable and accurate quantification. By comparing the hepatic lipid profiles in the I, HC, and HCI groups to that of the control, changes in lipid distribution under different metabolic conditions were examined statistically. The changes in hepatic lipidome in rabbits were compared with those in the serum reported in a previous study [26] to assess the differences in their lipid metabolism.

Experimental

Materials and reagents

Twenty-nine lipid standards were utilized to optimize the separation conditions for lipid analysis in this study: 12:0-lysophosphatidylcholine (LPC), 16:0-LPC, 14:0/16:0-PC, 15:0/15:0-PC, 16:0/16:0-PC, 18:0/18:1-PC, 14:0-lysophosphatidylethanolamine (LPE), 12:0/12:0-PE, 18:0/22:6-PE, 18:0-lysophosphatidic acid (LPA), 18:0/18:0-PA, 14:0-lysophosphatidylglycerol (LPG), 18:0-LPG, 15:0/15:0-PG, 18:0/18:0-PG, 16:0/18:2-phosphatidylinositol (PI), 14:0/14:0-phosphatidylserine (PS), 16:0/16:0-PS, $(18:1)_4$-cardiolipin (CL), d18:1/16:0-sphingomyelin (SM), d18:1/24:0-SM, d18:1/14:0-ceramide (Cer), d18:1/22:0-Cer, d18:1/12:0-monohexosylceramide (MHC), d18:1/18:0-MHC, d18:1/16:0-dihexosylceramide (DHC), 16:0/18:1-diglyceride (DG), 18:0/18:1-DG, and 18:0/18:0/18:1-triglyceride (TG) were purchased from Avanti Polar Lipids, Inc. (Alabaster, AL, USA) and Matreya, LLC. (Pleasant Gap, PA, USA). HPLC-grade H_2O, CH_3OH, isopropanol (IPA), and acetonitrile (ACN) were purchased from Avantor Performance Materials, Inc. (Center Valley, PA, USA), and $CHCl_3$ and methyl *tert*-butyl ether (MTBE) were obtained from Sigma-Aldrich Co., LLC (St. Louis, MO, USA).

Samples

Four groups of rabbits were grown under different metabolic states: healthy controls (C, $n=6$), inflammation by injecting 3 mL of 1 % carrageenan (I, $n=6$) per day for 3 weeks, high-cholesterol diet (HC, $n=5$) for 6 months, and high-cholesterol diet with inflammation by carrageenan (HCI, $n=5$) for 6 months. The hepatic tissue from each rabbit was obtained

and rinsed three times on a petri dish with ice-cold PBS solution (0.1 M). The PBS solution was decanted after each rinse. The washed tissue was minced into 2–3-mm-long pieces with scissors and lyophilized to dryness for 16 h. The dried samples were crushed into fine powder using a spatula.

Lipid extraction from samples

The protocols for lipid extraction were based on the Folch method modified with MTBE/CH_3OH, whose reproducibility had been validated in a previous paper [27]. For nontargeted lipid analysis by nLC-ESI-MS/MS, the hepatic tissue samples were pooled by group to a final weight of 10 mg (distributed equally between the samples), placed inside a 2-mL centrifugal tube, and mixed with 300 μL of CH_3OH. The mixture was placed in ice water for 10 min, followed by the sonication for 2 min in an ice bath to enhance lipid extraction, and 1000 μL of MTBE was added followed by vortexing for 1 h. Subsequently, 250 μL of HPLC-grade H_2O was added and centrifuged at 1000×*g* for 10 min to obtain distinct partitioning between the aqueous and organic layers. The upper organic layer was pipetted into a new 2-mL centrifugal tube. Three hundred microliters of CH_3OH was added to the remaining aqueous layer and vortexed again for 10 min followed by centrifugation at 1000×*g* for 10 min. The supernatant was pipetted, combined with the previously collected organic layer, and lyophilized to dryness with the lid open. The open top was wrapped with a 0.45-μm MillWrap PTFE membrane from Millipore (Bedford, MA, USA). The dried hepatic lipids were reconstituted in $CHCl_3/CH_3OH$ (1:1, *v*/*v*), diluted to a final concentration of 20 μg/μL in a solution of CH_3OH/ACN (9:1, *v*/*v*), and kept in a refrigerator at 4 °C.

For quantitative analysis by nUPLC-ESI-MS/MS, 10 mg of hepatic tissue from each individual sample was subjected to the same extraction procedure.

Nontargeted lipid identification using nLC-ESI-MS^n

A model LTQ Velos ion trap mass spectrometer from Thermo Scientific (San Jose, CA, USA) coupled with a 1200 capillary LC pump system with an autosampler from Agilent Technologies (Santa Clara, CA, USA) was employed for the identification of hepatic lipidome. For an analytical column, a silica capillary tube (360 μm O.D., 75 μm I.D.) was pulled by flame to make a sharp needle at one end and packed with a methanol slurry of Watcher ODS-P C18 particles (3 μm–100 Å) from Isu Industry Corp. (Seoul, South Korea) under N_2 gas at 1000 psi and then cut to a length of 6 cm. One end of a PEEK MicroCross from IDEX (Oak Harbor, WA, USA) was connected to the LC pump via a capillary tube, whereas the other three ends of the MicroCross were for the connection with a Pt wire (electric source), split flow valve, and analytical column. For lipidomic analysis, the extracted lipids were mixed with internal standard (IS, 13:0/13:0-PC) to the final concentration of 5 μg/μL and 500 fmol/μL for extracted hepatic lipids and IS, respectively, and a total of 2 μL of sample (10 μg of extracted hepatic lipids and 1 pmol of IS (15:0/15:0-PC)) was injected for each run to compensate the fluctuation of MS intensity. 13:0/13:0-PC was detected in both positive and negative ion modes in the forms of $[M+H]^+$ and $[M+HCO_2]^-$, respectively, where the collision-induced dissociation (CID) spectrum of $[M+H]^+$ was confirmed in MS^2 while that of in $[M+HCO_2]^-$ in MS^3. The lipidomic analysis was carried out in both positive and negative ion modes, separately, under a different elution gradient optimized for each ion mode. As a mixed modifier was used, the same types of mobile phases were utilized for both modes. Mobile phase A, which consisted of H_2O/ACN (9:1, *v*/*v*) with mixed modifiers (5 mM HCO_2NH_4 and 0.05 % NH_4OH), was utilized to load the sample into the analytical column at a flow rate of 600 nL/min for 10 min with the split flow valve off. Mobile phase B, which consisted of IPA/CH_3OH/ACN (6:2:2, *v*/*v*/*v*) with the same modifiers, was ramped to 40 % over 1 min with the split flow valve on at a pump flow rate of 10 μL/min, ramped to 80 % over 5 min, gradually increased to 100 % over 35 min, and maintained at 100 % for another 25 min in negative ion mode. Pressure tubing was attached to the split valve so that only 300 nL/min out of 10 μL/min was continuously eluted through the analytical column while the rest exited through the split flow valve. The high rate of pump flow set at 10 μL/min was used to decrease dwell time. In positive ion mode, mobile phase B was increased to 40 % over 1 min at a pump flow rate of 10 μL/min, increased to 80 % over 10 min, increased to 100 % over 20 min, and maintained at 100 % for 35 min. Once again, only 300 nL/min out of 10 μL/min was delivered to the column with the split flow valve open.

The range of the precursor scan was set at 350 to 1200 Da for both the positive and negative ion modes. The structures of all lipids except SM, Cer, and MHC were identified from the CID spectra in MS^2 at 40 % normalized collision energy. The ESI voltages were +3 and −4 kV in the positive and negative ion modes, respectively. PCs, PEs, DGs, and TGs were analyzed in MS^2 of positive ion mode, whereas PI, PG, PS, PA, and CL were identified in MS^2, and SM, Cer, and MHC were identified in MS^3 of negative ion mode since precursor ions of these three were detected as formate ($-HCO_2$) adducts. The structural identification of lipids was assisted by LiPilot, a computer-based algorithm designed for qualitative analysis using LTQ Velos [28].

Quantitative analysis using nUPLC-ESI-MS/MS

A nanoACQUITY UPLC from Waters (Milford, MA, USA) was coupled with a TSQ Vantage triple-stage quadrupole MS from Thermo Scientific and a 7-cm-long analytical column for nUPLC-ESI-MS/MS was prepared in the sample way as

above (75 μm I.D. packed with 3 μm–100 Å C18). The same mobile phase and modifiers were used, but the gradient elution conditions were different. The sample was loaded into the column for 5 min at a flow rate of 2 μL/min with mobile phase A with the split valve closed. The flow rate was then increased to 40 μL/min with the split valve open and 400 nL/min of the flow was delivered to the analytical column during elution. Mobile phase B was increased to 50 % over 0.1 min, 80 % over 3 min, and 100 % over 5 min and then maintained at 100 % for 12 min. Finally, equilibration was carried out using mobile phase A for 5 min. During elution, the flow rate of the analytical column was adjusted to 400 nL/min using the pressure tubing via the split valve. The analysis was carried out in SRM mode based on targeted product ions of all lipids, which were confirmed using lipid standards. For example, $[PCho+H]^+$ was set as the product ion for detecting all PCs and SMs; $[M+H-141]^+$ was used to detect PEs; $[M+NH_4\text{-}RCOONH_4]^+$ for DGs and TGs; $[RCOO]^-$ for PAs, PSs, PGs, PIs, and CLs; and $[dSGB]^+$ (dihydroxy sphingoid base) for Cers and MHCs. The detecting ion mode was alternated between positive and negative ion mode in order to analyze all lipids in a single run, saving analysis time, at a scan width of *m/z* 1.0, a scan time of 0.01 s, and an ESI voltage of 3 kV. The PCs, PE, DGs, TGs, SMs, Cers, and MHCs were analyzed in positive ion mode, whereas the others were analyzed in negative ion mode. The collision energy depended upon the lipid type: 40 V for PCs, SMs, DGs, and TGs; 20 V for PEs; 30 V for Cers, MHCs, DHCs, and THCs; and 35 V for PIs, PGs, and CLs. A total of 10 μg of extracted hepatic lipids along with 1 pmol of two types of IS, 13:0/13:0-PC for positive and 15:0/15:0-PG for negative ion mode, was injected for each run. Unlike the qualitative lipidomic analysis in the previous section, the quantitative analysis in SRM was carried out in MS^2 only, so the PG species was utilized as an additional IS in negative ion mode.

Results and discussion

The nontargeted hepatic lipidomic analysis was carried out with a pooled sample of control rabbits by data-dependent CID analysis of nLC-ESI-MS^n from separate positive and negative ion mode runs; the base peak chromatograms are shown in Fig. S1 of the Electronic supplementary material (ESM). A total of 346 hepatic lipids (66 PCs, 41 PEs, 21 DGs, 46 TGs, 15 PAs, 34 PSs, 30 PGs, 51 PIs, 3 CLs, 11 SMs, 17 Cers, and 11 MHCs) were identified from the CID experiments. Although most lipids were identified by MS/MS experiments, a couple of SL species with a relatively uncommon sphingoid base (d20:1) was identified by the MS^3 experiments (Fig. 1). The precursor ion of Fig. 1a was *m/z* 887.8 (t_r = 47.3 min) which was found to be the formate adduct ion $[M+HCO_2]^-$, and its first CID spectra showed a dominant fragment at *m/z* 827.8, which was 60 Da less than the precursor ion, indicating that the resulted MS^2 fragment was $[M-CH_3]^-$. The MS^3 experiment of *m/z* 827.8 is shown in Fig. 1a. The fragment ion at *m/z* 756.8 in Fig. 1a corresponds to the loss of $CH_2CHN(CH_3)_2$ from $[M-CH_3]^-$ and the peak at *m/z* 738.7 represents the additional loss of H_2O from $[M-CH_3-CH_2{=}CH\text{-}N(CH_3)_2]^-$. The fragment ions at *m/z* 367.5, 459.5, and 477.6 are the typical characteristic fragments generated from a fatty acyl chain; these peaks reflect the free carboxylate anion ($[RCOO]^-$)) of the fatty acyl chain 24:0 and the dissociation of the 24:0-fatty acid from $[M-CH_3]^-$ in the forms of carboxylic acid and ketene, respectively. These results support the structural identification of d20:1/24:0-SM and M represents the zwitterionic form of the SM lipids. For the case of Cer, a slightly different scheme was used to determine their structural information in Fig. 1b. A particular Cer species was detected as a formate adduct form at *m/z* 722.8 in precursor scan (t_r = 50.1 min) and the first CID

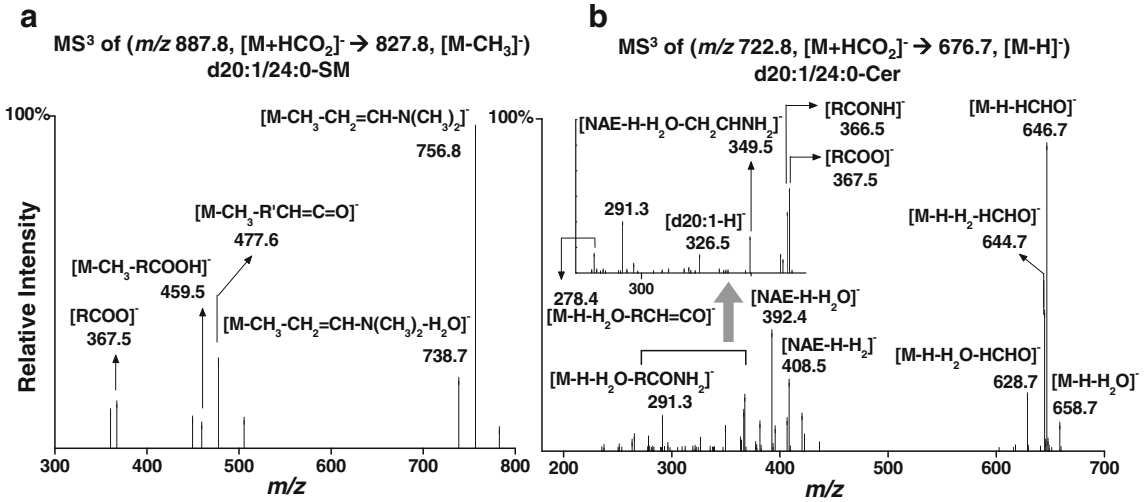

Fig. 1 MS^3 spectra of **a** d20:1/24:0-SM (t_r = 47.3 min) and **b** d20:1/24:0-Cer (t_r = 50.1 min) of the hepatic tissue of control rabbits from nontargeted lipid analysis using nLC-ESI-MS/MS

experiment resulted in product ions ($[M-H]^-$) at *m/z* 676.7, differing by 46 Da. The MS^3 experiment of *m/z* 676.7 resulted in the MS^3 spectra shown in Fig. 1b. Fragment ion (*m/z* 291.3) by the elimination of H_2O from the d20:1 chain and additional loss of the fatty acyl chain as a form of amide results in [M-H_2O-$RCONH_2$], of which identifies the fatty acyl chain as 24:0, and the other fragments at *m/z* = 366.5 and 367.5 in the expanded spectra shown in the inset are confirmed as $[RCONH]^-$ and $[RCOO]^-$, respectively. In addition, the deprotonated sphingoid base of d20:1 ($[d20:1-H]^-$) is observed at *m/z* 326.5. The loss of H_2O and H_2 from deprotonated N-acy-laminoethanol ($[NAE-H-H_2O]^-$ at *m/z* 392.4 and $[NAE-H-H_2]^-$ at *m/z* 408.5) further supports the presence of the d20:1-sphingoid base. The structures of other lipid classes were determined based on the fragment ions from CID spectra as listed in Table S1 of the ESM. The molecular structures of 304 lipids are listed in Table S2 in the ESM.

To explore lipid alteration under different metabolic conditions, all lipids identified from the nontargeted analysis were rapidly quantified by nUPLC coupled with triple-quadrupole MS using SRM. To achieve the high-throughput and high-speed quantitative analysis of a large number of lipids in a single LC run, a simple platform for relative quantitation based on SRM responses was established for the rapid detection of 306 lipids (304 hepatic lipids + 2 IS) using a 20-min separation; the general time frame required to detect each class of lipids is shown in Fig. 2. Instead of simultaneously scanning all lipids for detection during the entire 20-min period, each species was programmed for detection during an assigned 2-min time interval ($t_r \pm 1$ min) after confirming the retention time of each individual species (listed in ESM Table S2). This was done to maximize the number of collected data points for each lipid. Because the average peak width of most lipids was calculated to be 0.73 ± 0.02 min based on the bottom width, the 2-min intervals were sufficiently long to cover the relative uncertainty (approximately 2.03 % after 70 runs) in retention time. For instance, five SM species were detected from 10.0 to 11.7 min (based on retention time at peak maximum) during the nUPLC-ESI-MS/MS run, but each SM species was scanned for 2 min. Not all five SMs were scanned simultaneously because some of their detection durations overlapped, as shown in the upper right panel of Fig. 2. The overall detection duration of these five SMs ranged from 9.0 to 12.7 min. Thus, the lowest number of lipids added in the inclusion list of MS experiments and detected simultaneously was one species (t_r = 19.7–20 min), whereas the highest was 70 species (t_r = 7.3 min). As a majority of lipids eluted around 6–10 min, the number of lipids detected during this duration was relatively high. By utilizing the timetable established in Fig. 2, high-throughput and high-speed relative quantitation based on SRM responses can be achieved with a large number of lipids in a single run without repeating LC runs so long as the reproducibility in retention time is maintained. Thus, the SRM timetable in Fig. 2 was applied throughout the analysis.

The peak area of each individual lipid species was normalized by the peak area of IS and corrected by multiplying it by the volume of the dissolving solvent, which was added to the dried sample at the end of the extraction to adjust the extracted lipid concentration to 20 μg/μL. Table S2 in the ESM summarizes the corrected relative peak area ratios of all identified species with respect to those of the controls; each number written in parenthesis below the classes of lipids indicates the number of species quantified from each corresponding class. Each sample was analyzed three times, and the average value is listed in the table. The structures of the fatty acyl chains (with chain locations) of all lipids were identified in the nontargeted analysis from the peak intensities in the CID spectra, whereas the dominant product ions of $[PCho+H]^+$ (*m/z* 184) and $[M+H-141]^+$ were used in the SRM quantification for all PCs and PEs, respectively. Therefore, all isomers including regioisomers having the assigned *m/z* were detected together as one species, as listed in ESM Table S2 (e.g., 32:2-PC instead of 14:0/18:2-PC or 16:1/16:1-PC). As all 346 lipids were eluted within 20 min, isomers of PC and PE were detected as single peak instead of multiple peaks in SRM mode. For DG, PG, PI, PA, and PS lipids, where the product ions were fatty acyl chains so isomeric species could be

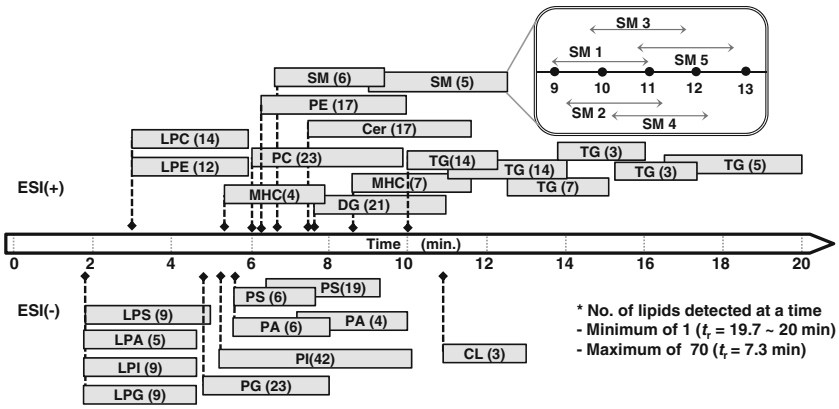

Fig. 2 Timetable for the rapid quantitative analysis of 306 lipids in SRM mode using nUPLC-ESI-MS/MS. The *numbers* indicate the total number of lipids detected from the corresponding classes

detected separately, the differences in retention times of isomeric species were mostly ranged between 0.0 and 0.3 s. Therefore, differentiation in retention times of isomers was not considered. Thus, even though 346 hepatic lipids were identified from the nontargeted lipid analysis, a total of 304 hepatic lipids were quantified by nUPLC-ESI-MS/MS. All confirmed isomers of PCs and PEs along with possible isomers of TGs from the nontargeted analysis are listed in Table S3 of the ESM. The expressed PC and PE species with the total carbon number of acyl chains less than 28 represent lysophospholipids (LPC and LPE, respectively.)

The relative abundance of each lipid within the corresponding lipid classes was calculated in percentages (e.g., relative peak area ratios of 18:2-LPC compared to the sum of the peak area ratios of all PCs) based on the SRM responses. Though the relative abundance in this work may not reflect the actual molar abundances, it will be referred as the relative SRM responses hereafter. If the calculated value was higher than the average abundance (100 %/ number of species quantified from each corresponding class), the species was considered to be relatively high-abundant in this study; these species are underlined in the "abun. %" column. The relative abundances of hepatic lipids were also directly compared with those of serum lipoprotein lipids from control rabbits from a previous study [26], in which the same rabbits were sacrificed to obtain serum samples. The species marked with asterisk (*) showed relatively high abundance in lipoproteins from serum. A majority of PCs (9 out of 10) and TGs (8 out of 9) that were relatively high-abundant in hepatic tissue were also relatively high-abundant in serum lipoproteins. This result can be explained by the fact that the liver is a major site for the synthesis of fatty acids and TG, and lipids are transported from the liver to other organs via the blood. This indicates that the origins of most PCs and TGs share a certain degree of similarity, even though the complete lipidome profile of these two sources might not be identical. We also observed a similarity among PEs, PAs, and PIs; approximately half of the high-abundant hepatic lipids were found to be high abundant in serum. The high abundances of hepatic DGs, PSs, and MHCs could not be compared to those of serum because serum DGs were not analyzed in the previous work, and only a single species from each class of PS and MHC was identified from serum.

Figure 3 shows the change in the total peak area of each lipid class among different metabolic states based on the variation in individual species that are high abundant in each class. Low-abundant species (listed in ESM Table S2) were grouped as "etc." category in each bar graph. In Fig. 3, the average peak areas of all species within the same class of lipids were summed together and their sum from controls was set as "1" for all classes of lipids. The relative alteration of summed lipids from the other three groups (I, HC, and HCI) with respect to controls is illustrated to demonstrate how each class of lipids is altered under different metabolic conditions, and the exact alteration ratios of individual species are listed in ESM Table S2. In addition, lipids with relatively high or moderate abundance from each class are shown together to briefly present how individual lipids increase or decrease under different conditions. In group I, the total lipidome levels did not change significantly for all classes of lipids; however, distinct increases among HCs and HCIs were clearly observed, implying that a high-cholesterol diet causes perturbation in lipid homeostasis, a marked feature of NAFLD. Dramatic increases of TGs in HC and HCI were easily observed, including those of extremely high-abundant TGs such as 50:1-TGs and 52:2-TGs (>2.7-fold in

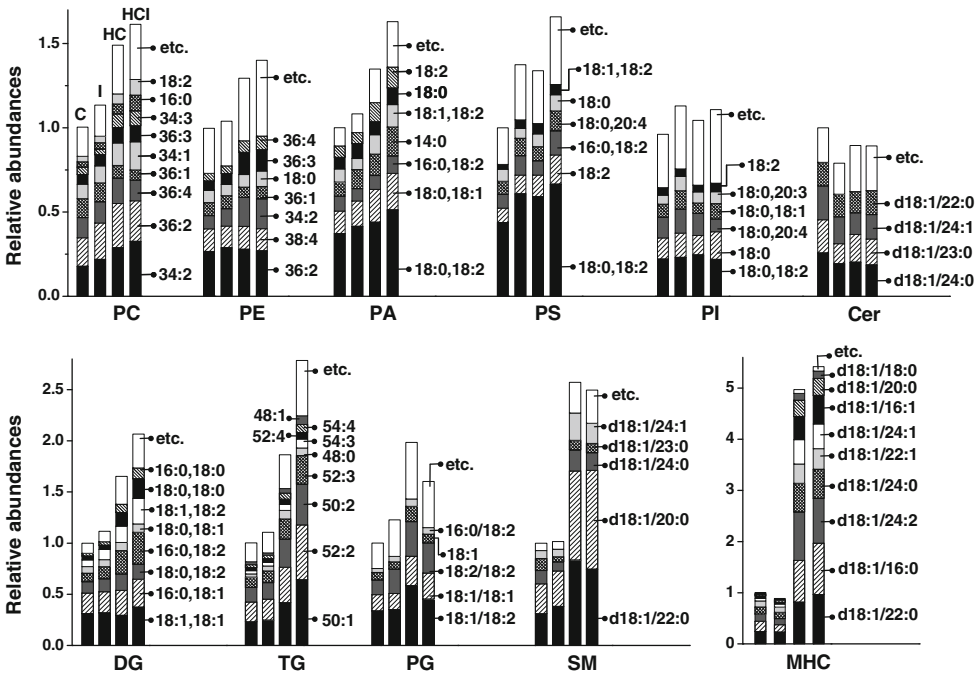

Fig. 3 Change in total lipidome under different metabolic states determined by nUPLC-ESI-MS/MS. The average peak areas of all species within the same groups were summed together by each class of lipids, and the sum of the peak areas of the controls was set into "1" for all classes of lipids

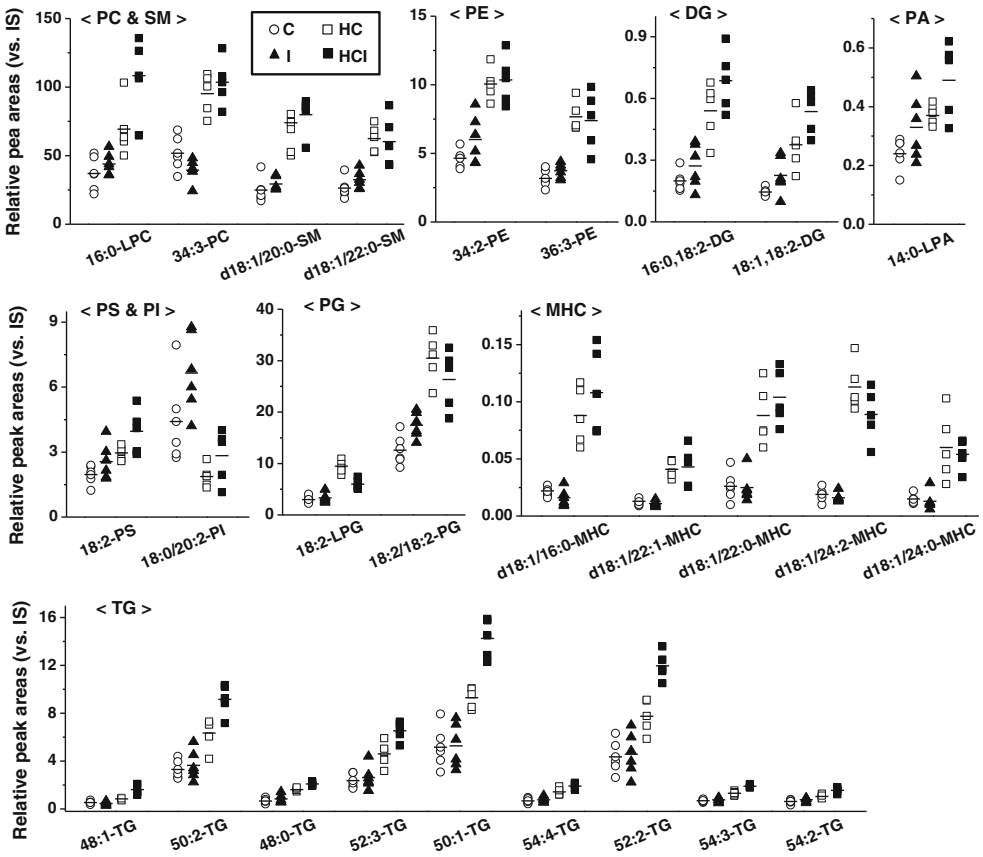

Fig. 4 Relative peak areas of high-abundant hepatic lipids with significant alternations (>2-fold and p value < 0.01) under different metabolic states

HCI). As the accumulation of TGs is a hallmark feature of obesity and NAFLD, the high-cholesterol diet is deduced to promote fatty liver, and the promotion is more severe when combined with inflammation. On the other hand, as no class of hepatic lipidome changed significantly in group I, inflammation alone does not appear to cause noticeable perturbation in lipid metabolism nor is it likely correlated with NAFLD.

The total concentrations of DGs observed in the HC and HCI groups (Fig. 3) were increased by approximately 1.6- and 2-fold, respectively. The causes for the accumulation of DG may be multifactorial and may include increased fatty acid uptake by the liver, increased hepatic de novo lipogenesis (conversion of acetyl-CoA to fatty acid), or mitochondrial dysfunction [29]. Mitochondrial dysfunction is associated with hepatic insulin resistance, which is one of the many common manifestations of NAFLD. Insulin resistance disrupts and impairs lipid metabolism by enhancing lipid accumulation [30], which was observed in this study; the majority of lipids increased simultaneously with TGs in the HC and HCI groups. As DGs accumulated in the HC and HCI groups, we again concluded that a high-cholesterol diet contributes to the development of NAFLD. However, although the levels of DGs increased by 1.6-fold and 2-fold in the HC and HCI groups, respectively, extremely high-abundant species such as 18:1/18:1-DG and 16:0/18:1-DG did not change much, and DGs with (16:0,18:2), (18:1,18:2), and (18:0,18:0) in particular, showed remarkable increases. These results indicate that the increase in DG lipidome is likely caused by the increase in relatively moderate-abundant or low-abundant DG species. This illustrates that not all lipids are necessarily influenced in the same way or to the same degree by metabolic factors during disease development.

In addition to DGs and TGs, various classes of lipids increased in the HC and HCI groups, including SMs; increases in relatively high-abundant d18:1/22:0-SM and d18:1/20:0-SM in the HC and HCI groups are clearly observed in Fig. 3. The most significant increase was observed for MHCs, which were increased by approximately 5-fold in both the HC and HCI groups. Increases in all MHCs, both high abundant and low abundant, were clearly observed. However, as MHC level once again remained unchanged in group I, the increase in MHC appears to be caused solely by the high-cholesterol diet. Many studies have already reported an increase in TGs with fatty liver development; however, the results of this study suggest that MHCs are also increased dramatically, if not more than TGs. The increases in complex sphingolipids such as MHCs and SMs are associated with ceramides as sphingolipids are converted from ceramides via de novo synthesis by various enzymatic reactions [31].

As changes in high-abundant species have more significant effects on total lipidome levels compared to changes in low-abundant species, the changes in the peak areas of high-

Table 1 Hepatic lipids with significant differences (in bold, >3-fold; $p<0.01$) compared to healthy controls determined by nUPLC-ESI-MS/MS. Abundance (%) in italics indicates relatively high-abundant species within the corresponding lipid classes

Classes	Molecular species	*m/z*	I/C	HC/C	HCI/C	Abundance (%)	Classes	Molecular species	*m/z*	I/C	HC/C	HCI/C	Abundance (%)
PC	14:0	518.4	0.89 ± 0.07	**3.03 ± 0.52**	**5.48 ± 0.45**	0.01	PG	14:0	455.4	1.73 ± 0.17	**3.73 ± 0.41**	**7.17 ± 0.68**	0.01
	22:4	572.4	2.69 ± 0.70	**4.37 ± 0.57**	**6.31 ± 0.45**	0.00		16:1	481.3	1.38 ± 0.14	**4.67 ± 0.56**	**3.63 ± 0.40**	0.09
	20:1	550.4	0.99 ± 0.07	2.38 ± 0.35	**3.17 ± 0.27**	0.03		18:2	507.3	1.65 ± 0.20	**3.59 ± 0.37**	2.11 ± 0.19	*3.33*
	32:0	730.6	1.36 ± 0.12	2.20 ± 0.20	**4.16 ± 0.52**	0.44		14:0/18:2	717.6	2.13 ± 0.24	2.76 ± 0.41	**3.44 ± 0.46**	0.04
PE	16:1	452.4	1.16 ± 0.09	2.55 ± 0.53	**4.20 ± 0.39**	0.05		16:1/16:1	717.6	1.42 ± 0.21	**3.43 ± 0.58**	**3.29 ± 0.39**	0.2
	36:5	738.6	1.02 ± 0.12	2.99 ± 0.33	**3.06 ± 0.32**	0.98		14:0/18:1	719.6	1.57 ± 0.24	**4.47 ± 0.67**	**4.18 ± 0.33**	0.07
	34:3	714.8	1.12 ± 0.13	1.98 ± 0.24	**3.57 ± 0.40**	0.73		16:0/16:1	719.6	1.21 ± 0.16	**3.73 ± 0.58**	**3.13 ± 0.39**	0.19
DG	16:0, 18:2	610.6	1.39 ± 0.17	2.70 ± 0.34	**3.67 ± 0.36**	*8.40*	PA	18:0/22:5	749.5	0.98 ± 0.27	**6.89 ± 1.25**	**4.27 ± 0.77**	0.12
	16:0, 16:0	586.4	1.33 ± 0.22	**3.21 ± 0.67**	**3.92 ± 0.84**	1.29		18:2/20:2	723.6	1.52 ± 0.63	**3.51 ± 0.64**	**5.08 ± 0.89**	0.86
	18:1, 20:4	660.6	1.05 ± 0.21	2.87 ± 0.71	**3.31 ± 0.67**	0.62	SM	d18:1/16:1	701.7	1.22 ± 0.12	**8.43 ± 0.86**	**9.73 ± 1.00**	0.14
	16:0, 22:5	660.6	1.07 ± 0.18	2.80 ± 0.54	**3.52 ± 0.71**	0.42		d18:1/16:0	703.7	1.39 ± 0.19	**5.75 ± 0.80**	**6.50 ± 0.83**	2.58
	18:1, 18:2	636.6	1.55 ± 0.22	2.56 ± 0.41	**3.95 ± 0.57**	*6.34*		d18:0/16:0	705.7	0.89 ± 0.09	**10.26 ± 1.07**	**12.21 ± 1.26**	0.40
	16:0, 20:3	636.6	1.02 ± 0.14	2.77 ± 0.57	**3.84 ± 0.72**	0.37		d18:1/20:0	759.8	1.18 ± 0.08	2.97 ± 0.25	**3.30 ± 0.29**	*29.32*
	18:0, 18:0	642.7	1.07 ± 0.12	**3.40 ± 0.42**	**4.93 ± 0.58**	3.92		d18:1/24:1	813.8	0.96 ± 0.11	**3.47 ± 0.36**	2.55 ± 0.29	7.69
TG	44:0	768.8	1.04 ± 0.30	2.28 ± 0.60	**4.11 ± 0.78**	0.17	Cer	d18:1/16:1	536.6	1.13 ± 0.17	**10.15 ± 1.12**	**12.64 ± 2.72**	0.04
	46:0	796.8	1.21 ± 0.30	2.36 ± 0.51	**3.22 ± 0.49**	0.97		d18:1/16:0	538.6	1.64 ± 0.53	**4.32 ± 0.49**	**10.48 ± 1.69**	0.04
	48:1	822.8	0.86 ± 0.08	1.55 ± 0.14	**3.01 ± 0.26**	*2.79**		d18:1/18:1	564.6	1.59 ± 0.27	2.70 ± 0.46	**3.21 ± 0.60**	0.04
	48:0	824.9	1.26 ± 0.40	2.97 ± 0.39	**3.14 ± 0.57**	*3.84*	MHC	d18:1/16:1	698.6	0.78 ± 0.26	**9.64 ± 3.40**	**11.9 ± 3.83**	4.71
	54:1	906.8	1.18 ± 0.12	2.50 ± 0.30	**3.50 ± 0.47**	0.72		d18:1/16:0	700.6	0.74 ± 0.23	**4.09 ± 1.35**	**5.03 ± 1.56**	*19.96*
	54:0	908.9	1.55 ± 0.22	**3.14 ± 0.36**	**3.53 ± 0.59**	0.14		d18:1/18:1	726.6	1.12 ± 0.32	**6.57 ± 1.85**	**7.94 ± 2.33**	0.33
	56:1	934.8	0.91 ± 0.13	2.31 ± 0.39	**4.18 ± 0.78**	0.01		d18:1/18:0	728.6	1.05 ± 0.24	**6.32 ± 1.37**	**6.83 ± 1.58**	2.08
	58:1	962.8	1.00 ± 0.18	2.89 ± 0.45	**4.08 ± 0.53**	0.01		d18:1/20:1	754.5	1.27 ± 0.25	**7.47 ± 1.49**	**8.78 ± 1.89**	0.70
CL	$(18:1, 18:2)_2$	725.8	0.94 ± 0.23	**4.03 ± 0.83**	**4.78 ± 1.01**	6.93		d18:1/20:0	756.6	1.20 ± 0.22	**10.02 ± 1.92**	**10.96 ± 3.10**	3.18
PI	16:0/20:5	855.5	1.98 ± 0.45	**3.42 ± 0.66**	**5.85 ± 0.91**	0.01		d18:1/22:1	782.6	0.86 ± 0.11	**3.25 ± 0.50**	**3.46 ± 0.64**	*11.60*
PS	18:1	522.3	1.27 ± 0.15	2.58 ± 0.31	**3.44 ± 0.37**	1.48		d18:1/24:2	808.5	0.83 ± 0.12	**6.72 ± 0.94**	**6.21 ± 0.86**	*14.08*
	20:3	546.3	1.17 ± 0.16	1.73 ± 0.26	**3.35 ± 0.86**	0.51		d18:1/22:0	784.6	0.95 ± 0.14	**3.37 ± 0.59**	**3.98 ± 0.63**	*24.21*
	18:1/18:1	786.6	2.08 ± 0.54	2.76 ± 0.78	**4.19 ± 0.93**	0.30		d18:1/24:1	810.6	1.14 ± 0.17	**9.02 ± 1.56**	**9.10 ± 1.91**	5.28
	18:2/20:1	812.6	2.68 ± 0.56	2.71 ± 0.51	**3.43 ± 0.58**	0.42		d18:1/24:0	812.6	0.89 ± 0.13	**4.04 ± 0.61**	**4.13 ± 0.67**	*13.89*

abundant species were inspected closely. The lipid species underlined in ESM Table S2 are high-abundant species based on the species identified from the control group. Among them, high-abundant species showing greater than 2-fold differences in peak area ratio ($p < 0.01$) are indicated in bold in Fig. 4, where they are plotted with the relative peak area (vs. IS) to illustrate the individual peak area ratios of all samples. Unlike other classes of lipids, in which only a few high-abundant lipids showed significant changes, all nine high-abundant TGs and five MHCs increased significantly in the HCI group. However, as not a single high-abundant species was significantly altered in group I, inflammation alone does not seem to have any significant effect on the hepatic lipidome profile, even though inflammation combined with a high-cholesterol diet (HCI group) causes dramatic changes. The dramatic elevation in the HC-treated groups is easily observed in the MHCs, particularly because none of the peak area ratios overlapped with those of the HC and HCI groups.

Hepatic lipid species including low-abundant species that were significantly altered under metabolic conditions were examined further by screening with the stringency (>3-folds and $p < 0.01$; Table 1). A total of 32 and 54 lipids were increased significantly in the HC and HCI groups, respectively, whereas no species met the abovementioned criteria in group I. All 11 MHCs increased significantly in the HC and HCI groups, and a number of species from DG, TG, PG, and SM did as well.

A *Z*-score heat map based on the SRM quantification of all 304 hepatic lipids is shown in Fig. S2 of the ESM; the map well reflects the aforementioned observations regarding lipids. Discussion regarding the *Z*-score heat map is described in the ESM.

The changes in the peak area ratios of lipids from hepatic tissue under HC and HCI conditions were compared with those from serum lipoproteins reported previously [26] (Fig. 5 and ESM Fig. S3). Figure 5 is the comparison of the relative changes of selected lipids that showed significant changes in the liver, whereas ESM Fig. S3 is based on lipid species that showed large changes in HDL or LDL. Data for serum lipids were adapted from Table S2 of the ESM of [26] with permission from Elsevier Publishers. In Fig. 5, all TGs that were upregulated by a significant degree (>3-fold, $p < 0.01$) in hepatic tissue (black) under a high-

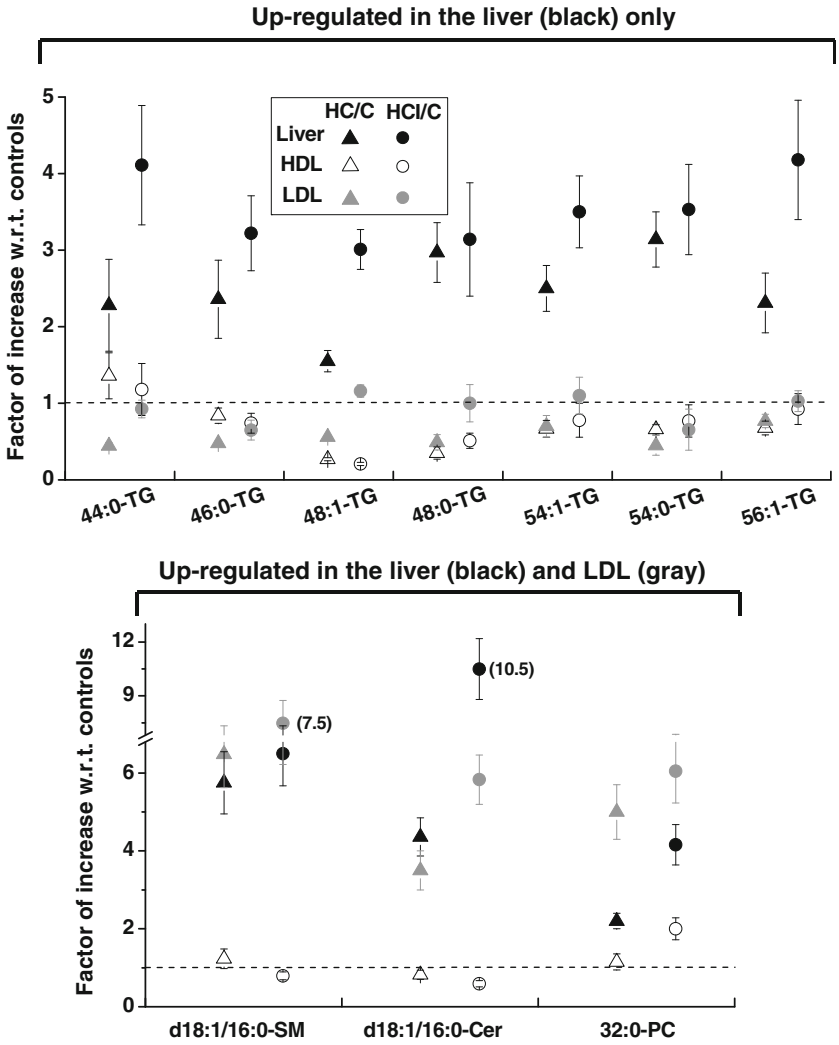

Fig. 5 Relative peak area ratios of lipids from hepatic tissue and lipoproteins of serum. The species that showed significant changes in hepatic tissue (>3-fold and p value < 0.01) are selected (species from Table 1)

cholesterol diet were regulated differently in HDL (open) and LDL (gray), by either decreasing or remaining unchanged. In ESM Fig. S3, 54:7-TG showed the same trend once again as it increased only in hepatic tissue. Unlike the aforementioned TG species, 52:5-TG and 52:4-TG in ESM Fig. S3 increasing in LDL in addition to in hepatic tissue, however, the 4.9–6.6-fold changes observed for lipoproteins are not considered significant because many lipids from HDL and LDL showed greater than 10-fold changes. Overall, lipoproteinic TGs either decreased or increased slightly, whereas hepatic TGs increased significantly. This phenomenon can be explained by the pathway of TGs; even though insulin resistance is purported to increase TG secretion, TGs that are synthesized in hepatic tissue are excessively accumulated in hepatic tissue along with fatty acids, leading to ER stress in the liver. Eventually, apolipoprotein B (ApoB) goes through degradation and mutation and decreases TG secretion via VLDL [18]. On the other hand, hepatic and serum 32:0-PC in Fig. 5 exhibit a similar trend by increasing under a high-cholesterol diet, and serum d18:1/16:0-SM and d18:1/16:0-Cer from LDL increased in the HC and HCI groups, as did hepatic lipids. In ESM Fig. S3, the PLs that showed significant changes in the lipoproteins (>10-fold and $p < 0.01$) did not show significant changes in hepatic tissue. A few PCs, 18:0/18:2-PS, 18:0-LPA, and all PIs were upregulated only in LDL; they were either slightly increased (<1.7-fold) or decreased in the liver. On the other hand, some lipids were simultaneously upregulated in both LDL (4.9–45-fold) and liver (2–2.9-fold), as illustrated in the bottom panel of ESM Fig. S3. Even though the serum and hepatic tissue were obtained from the same individuals, not only the profile of serum lipidome but also the pattern in alterations of lipidome level was different from those of hepatic tissue, dependent on the classes or fatty acyl chains of lipids.

Conclusion

This study introduces an analytical platform consisting of by nUPLC-ESI-MS/MS with SRM for the high-throughput and rapid quantification of more than 300 hepatic lipids that requires only 20 min. The hepatic lipidome profile of rabbits under NAFLD-inducing metabolic conditions was investigated, and a high-cholesterol diet was discovered to significantly perturb the hepatic lipidome, especially under the HCI group. This was observed in a previous study based on lipids from serum lipoproteins; the lipids from HDL and LDL exhibited the most significant changes in the HC and HCI groups. As the two classes of lipids (DGs and TGs) were significantly elevated in the HC and HCI groups, a high-cholesterol diet is presumed to be correlated with NALFD. The accumulation of DG is known to be associated with insulin resistance, which enhances lipid accumulation in the liver. With increased fatty acid uptake by the liver, the amount of fatty acid available for esterification of lipids is increased. Thus, DGs and TGs along with various classes of lipids including PLs were generally increased in the HC and HCI groups. In this study, apoptosis-inducing Cers were slightly decreased in hepatic tissue in the HC and HCI groups, whereas mitogenic SMs and MHCs were significantly increased. The increase in mitogenic lipids is also believed to contribute to the increases of other classes of lipids by accelerating cell proliferation. As these mitogenic SMs and MHCs did not change much in group I, other classes of lipids did not exhibit any significant increase. The most noticeable changes in lipids were observed in TGs and MHCs. Particularly in the HCI group, all of the relatively high-abundant TGs and MHCs significantly increased (>2-fold with $p < 0.01$). However, a slightly lower number of high-abundant TGs increased significantly in the HC group, indicating that a high-cholesterol diet with inflammation perturbs lipid metabolism to a larger degree than a high-cholesterol diet alone. On the other hand, inflammation itself does not seem to have a noticeable influence on hepatic lipids.

Acknowledgments This study was supported by a grant (NRF-2015R1A2A1A01004677) from the National Research Foundation of Korea and in part by a grant (NRF-2013M3A9B6046413) from the Bio & Medical Technology Development Program through the NRF funded by the Ministry of Science, ICT, & Future Planning.

Compliance with ethical standards Animal experiments complied with the Korea University Animal Science Rules and the protocols were approved by the Korea University Institutional Animal Care and Use Committee.

Conflict of interest The authors declare that they have no competing interests.

References

1. Brouwers JFHM, Vernooji EAAN, Tielens AGM, van Golde LMG. J Lipid Res. 1999;40:164.
2. Wright MM, Howe AG, Zaremberg V. Biochem Cell Biol. 2004;82:18.
3. Grundy SM, Cleeman JI, Daniels SR, Donato KA, Eckel RH, Franklin BA, et al. Circulation. 2005;112:2735.
4. Liu Y-Y, Hill RA, Li Y-T. Anti Cancer Agents Med Chem. 2012;12:340.
5. Nikolova-Karakashian MN, Rozenova KA. Adv Exp Med Biol. 2010;688:86.
6. Cajka T, Fiehn O. TrAC Trends Anal Chem. 2014;61:192.
7. Bang DY, Moon MH. J Chromatogr A. 2013;1310:82.
8. Moon MH. Mass Spectrom Lett. 2014;5:1.
9. Byeon SK, Lee JY, Lim S, Choi D, Moon MH. J Chromatogr A. 2012;1270:246.
10. Lee JY, Byeon SK, Moon MH. Anal Chem. 2015;87:1266.
11. Min HK, Lim S, Chung BC, Moon MH. Anal Bioanal Chem. 2011;399:823.
12. Byeon SK, Lee JY, Lee J-S, Moon MH. J Chromatogr A. 2015;1381:132.
13. Byeon SK, Kim JY, Lee J-S, Moon MH. Anal Bioanal Chem. 2016;408:2265.
14. Paschos P, Paletas K. Hippokratia. 2009;13:9.
15. Haga Y, Kanda T, Sasaki R, Nakamura M, Nakamoto S, Yokosuka O. World J Gastroenterol. 2015;21:12989.

16. Yu AS, Keeffe EB. Rev Gastroenterol Disord. 2002;2:11.
17. Yu S, Matsusue K, Kashireddy P, Cao WQ, Yeldandi V, Yeldandi AV, et al. J Biol Chem. 2003;278:498.
18. Koo SH. Clin Mol Hepatol. 2013;19:210.
19. James O, Day C. Lancet. 1999;353:1634.
20. Comhair TM, Garcia Caraballo SC, Dejong CH, Lames WH, Köhler SE. Nutr Metab. 2011;8:4.
21. Kerr TA, Davison NO. Hepatology. 2012;56:1995.
22. Donnelly KL, Smith CI, Schwarzenberg SJ, Jessurun J, Boldt MD, Parks EJ. J Clin Invest. 2005;115:1343.
23. Gordon DL, Ivanova PT, Myers DS, McIntyre JO, VanSaun MN, Wright JK, et al. PLoS One. 2011;6:e22775.
24. Puri P, Baillie RA, Wiest MM, Mirshahi F, Choudhury J, Cheung O, et al. Hepatology. 2007;46:1081.
25. Malhi H, Gores GJ. Semin Liver Dis. 2008;28:360.
26. Byeon SK, Kim JY, Lee JY, Chung BC, Seo HS, Moon MH. J Chromatogr A. 2015;1405:140.
27. Byeon SK, Lee JY, Moon MH. Analyst. 2012;138:451.
28. Lim S, Byeon SK, Lee JY, Moon MH. J Mass Spectrom. 2012;47:1004.
29. Jourayvas FR, Shulman GI. Cell Metab. 2012;15:574.
30. Qureshi K, Abrams GA. World J Gastroenterol. 2007;13:3540.
31. Claus RA, Dorer MJ, Bunck AC, Deigner HP. Curr Med Chem. 2009;16:1978.